Preparation of lipid nanoparticles by micro-mixer Process simulation and experimental study

Bing Li[1,a], Hao Miao[2] and Zhenbo Tong[1*]

[1] Center for Simulation and Modelling of Particulate Systems, Southeast University-Monash University Joint Research Institute, Suzhou, Jiangsu, PR China
[2]ARC Research Hub for Computational Particle Technology, Department of Chemical Engineering, Monash University, Clayton, Vic 3800, Australia

Abstract. Controlling the sizes of liposomes is critical in drug delivery systems because it directly influences their cellular uptake, transportation, and accumulation behaviour. Although micro-mixer has frequently been employed when synthesizing nano-sized liposomes, little is known regarding how flow characteristics determine liposome formation. The mixing performance of a three-dimensional micromixer with a herringbone groove structure was studied by numerical analysis, and its structure was optimized. The model was verified by simulation and experiment. In the herringbone groove structure, excellent mixing index can be achieved by split-recombination and chaotic advection mechanism. The results show that the mixing index increases with the increase of Reynolds number, and the mixing is very sensitive to the shape of the groove, which can be used for mixing control in microdevices.

1. Introduction

In the last decade, microfluidic devices have become increasingly prevalent in medical diagnostics, chemical analysis, drug development, and delivery due to their rapid mixing, continuous flow, and controllability [1, 2]. These devices have also enabled new approaches in medication delivery and drug research [3]. The therapeutic efficacy of nanomedicine is affected by its size. Large-sized nanomedicines are often captured and filtered out by the spleen's reticulum. Conversely, nanodrugs smaller than 10 nm are cleared by the lymphatic system. Size-controlled nanomedicines can effectively accumulate in the target organ and produce high therapeutic efficacy. Therefore, appropriately sized nanomedicines are expected to enable particle size-dependent drug delivery systems. Despite decades of development, traditional methods of LNPs preparation are difficult to precisely control the size of LNPs. For instance, LNPs sizes are adjusted in 5-10 nm intervals. To improve the precision of size control, new methods of LNPs preparation are being developed. Therefore, precise control of particle size is necessary for the development of next-generation nanomedicines.

Microfluidics enables precise control over processes such as mixing, droplet formation, and nanoprecipitation, which is not possible with conventional methods[4]. These devices have a wide range of applications, including material creation, biosensing, tissue engineering, and microelectronics. They can be made from various materials such as polymers, glass, silicon, or paper. Over the last two decades, research into nanomedicine has increased significantly due to advancements in soft lithography techniques and equipment design. These include flow focus generators, staggered herringbone micromixers, and hydrodynamic flow focusers [5, 6]. Microfluidic technology is currently mainly utilised for mixing and stirring two distinct liquids. The micro-mixer channel's small size causes the liquid to primarily impinge through the diffusion process, resulting in primarily laminar fluid flow. A 2008 study compared flow-focused microfluidic synthesis of polymer nanoparticles with native synthesis. The study found that microfluidics produces nanoparticles with smaller size distributions, higher encapsulation efficiencies, and drug loading, as well as slower release rates [7]. This demonstrates the advantages of microfluidics in nanoparticle synthesis.

However, the challenge remains: how to optimise the micro-mixer channel to achieve better mixing of the liquid in a shorter distance from the channel. A number of studies have shown that the faster the mixing rate, the smaller the size of the resulting lipid nanoparticles, which are more suitable for drug delivery. Maeki et al. (year) investigated the formation behaviour of lipid nanoparticles (LNP) in a microfluidic device with a staggered herringbone micro-mixer (SHM) structure. Ripoll et al. (year) studied the chip structure and flow state of the mixing process, which have a direct influence on the size, polydispersity index (PDI), and packaging of LNP [8]. The paper demonstrates the fundamental role of SHM in LNP formation by identifying the factors that limit the number of SHM cycles and the influence of flow rate conditions [6]. The number of SHM cycles and the

* Corresponding author: ztong@seu.edu.cn
a 992631164@qq.com

position of the first SHM are as crucial as the flow rate conditions in producing small-sized LNPs. The paper suggests that controlling the mixing speed and distance, as well as the critical concentration, are key factors in controlling the size of the LNPs [9]. Mixing is a complex process that involves various scale phenomena, such as flow advection at 10μm, liquid diffusivity at 1 nm, and chemical reactions at 0.1 nm [10]..

2 Model development

2.1.Micromixer structure

This section briefly introduces our proposed micromixer geometry diagram and the corresponding diagram. Figure 1a shows the SHM serpentine multicycle structure, which consists of 16 SHM cycle structures with 12 fins each, a shape similar to several types used by Stroock et al [11]. Figure 1b shows its specific structure diagram. There are 7 variables: a,b,w,h,s,f mixer According to these variables, the optimal S-type multi-cycle SHM micromixer structure can be obtained. The cross-sectional dimensions of the channel are 200μm x 79μm. The whole three-dimensional serpentine SHM groove structure is channelled into chaotic advection to improve the mixing efficiency.

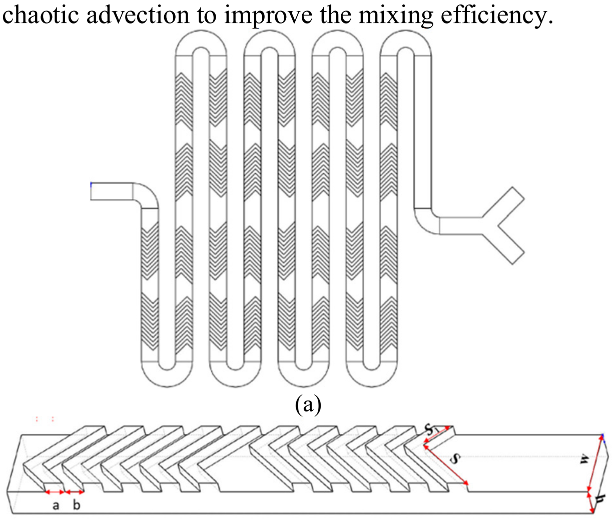

Fig. 1. Schematic diagram of microfluidic structure.

2.2. Test and simulation methods

To conduct the experimental research, an optical microscope (SAGA), a digital camera (Lycra), and a flow pump were used. The micromixer chip had two inlets connected to two 5ml syringes of the flow pump. Piccin et al. used a similar experimental setup, although they employed a micromixer to prepare the droplets, the setup was otherwise identical. To study the flow and mixing process and compare it with simulation results, this study used two fluids: deionized water and anhydrous ethanol. water $\rho_{Water} = 998.0kg \cdot m^{-3}$; $\mu_{Water} = 0.001kg \cdot m^{-1} \cdot s^{-1}$;) ethyl alcohol$\rho_e = 789.0kg \cdot m^{-3}$; $\mu_e = 0.0012kg \cdot m^{-1} \cdot s^{-1}$) , Considering the convenience of observing the diffusion process, Rhodamine fluorescent stain was used to stain the ethanol, and the ratio of Rhodamine stain was 1mg/ml. Since the process is a continuous process, OBS software is used to record the process after the system is stabilized, and Leica camera takes photos of it. The structure diagram is shown in Figure 2:

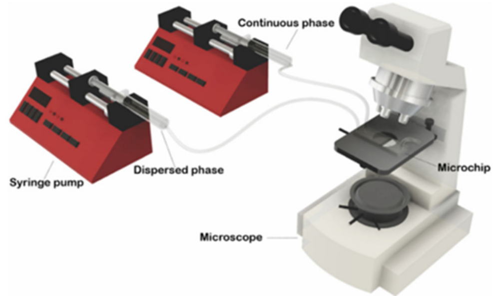

Fig. 2. Experimental structure diagram.

2.3. Computation fluidic dynamics simulation

In this study, Fluent 20.0 (ANSYS, USA), a commercial fluid simulation software based on finite volume method, was selected to completed numerical simulation. The cross-sectional feature size of the designed microchannel is of micron scale, which can be considered to apply the continuity equation with N-S equation. Steady, incompressible, and Newtonian flow is considered in the microchannel. In our case, the well-known Semi-Implicit Pressure-Linked Equation (SIMPLE) algorithm was used to solve the equation, and second order upwind numerical schemes was used.

The specific equation is as follows:

Equation of continuity:

$$\nabla \cdot U = 0 \tag{1}$$

Navies stokes equation:

$$\partial(U)/\partial t+\rho((V \cdot \nabla))\ U=-\nabla P+\mu\nabla\hat{}2\ U \tag{2}$$

Where U is the flow rate of the fluid, m/s; μ is the liquid viscosity, Pa·s; P is the pressure, Pa; C is the concentration of the compound, mol/l; D is the component diffusion coefficient, m^2/s.

To study the phenomenon of mixing in a micromixer used for preparing LNP, anhydrous ethanol and deionized water were selected as the fluid as the working fluid. The

molar concentrations of ethanol at inlet 1 and inlet 2 are 0 mol/m^3 and 1 mol/m^3, respectively. The boundary conditions are set to constant inlet velocity, steady state outlet static pressure is 0, wall no slip, and gravity is set to 9.8m^2/s. Fixed speed set for two entrances. The properties of these fluids at 20 °C are listed in Table 1

Table 1. Fluid characteristics at room temperature.

Fluid	Density (Kg/$\mathbf{m^3}$)	Viscosity (Pa ·s)	Diffusivity ($\mathbf{m^2}$/s)
Water	9.98×10^3	0.9×10^{-3}	1.2×10^{-9}
Ethanol	7.89×10^3	1.2×10^{-3}	1.2×10^{-9}

Except where Mixing performance was assessed using a mixing index, defined as:

$$\sigma_M = \sqrt{\frac{1}{N}\sum(c_i - \bar{c}_M)^2} \quad (3)$$

$$M_i = 1 - \sqrt{\frac{\sigma^2}{\sigma_{max}^2}} \quad (4)$$

where σ identifies the change in concentration per cross-section, σ_M is the maximum variance over the range of the data, N is the number of nodes within the cross-section, c_i is the mass fraction at sampling point i, $\bar{c}_M$ is the optimal mixing fraction (0.4417 mol/m^3), and M_i is the mixing index. A mixing index of one indicates complete mixing and zero indicates no mixing. The values of the sampling points were obtained by interpolation with the values of neighboring gold acid units.

The two inlets have a concentration of 0 and 1, respectively, while flowing into the same volume, so the optimal mixing mass fraction value is 0.4417.

Re has a relatively large influence on the fluid flow and in this paper, we need to study the mixing index through the Reynolds number, so it is defined in this paper as follows:

$$Re = \frac{\rho V D}{\mu} \quad (5)$$

where D and μ represent the hydraulic diameter of the micromixer and the dynamic viscosity of the fluid respectively.

3. Results and discussion

3.1. Numerical analysis

To determine the optimal number of grids, it has been determined that the grids are not relevant for solving this scheme, a grid-independence determination has been carried out.7 different number of grids in the grid number from 5.3×10^5 to 1×10^8 have been tested to evaluate the velocity magnitude distribution along the SHM microchannel by gradually increasing the number of nodes. The test results are shown in Fig. 3, from which the velocity test has a negligible effect on the accuracy of the results at nodes more than 3.37×10^5 grids, and the grid 3.37×10^5 nodes were selected as the optimal nodes, so this grid refinement was chosen for this study to carry out the next simulation. An example of the mesh system is shown in Fig. 2b, using Fluent meshing unstructured mesh. The notches as well as the corners are encrypted as shown in Fig. 3.

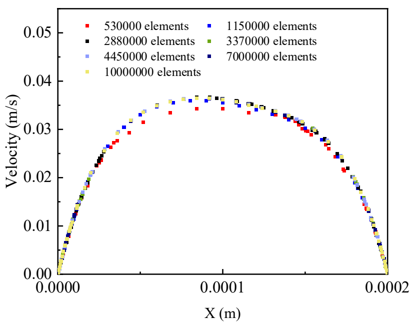

Fig. 3. Grid sensitivity analysis to the channel velocity.

3.2.Model validation

The present calculations were qualitatively compared with Stroock's experimental results and Kwang's simulations [11, 12]. For the variance distribution, it is shown in Figure 4. The fluids considered in their experimental analysis were water and a solution of 80% glycerol and 20% water. The viscosity of the glycerol/water solution was $6.7\times 10^{-2} kg\cdot m^{-1}\cdot s^{-1}$, while ethanol was $1.2\times10^{-3}\ kg\cdot m^{-1}\cdot s^{-1}$. However, the current numerical calculations and optimizations were performed using water and dewatered ethanol for Pe=2.0×10^3. The mixer used for the experiments of Stroock et al. Some of the data such as the spacing of each SHM cycle and the spacing of half a cycle are not known due to lack of details of the structural data given in the literature. The spacings used in that study were 150μm and 50μm, respectively. therefore, the differences in Fig. 4 are due to differences in geometry and working fluid. To illustrate the effect of fluid mobility within the microchannel as on mixing, the results of the numerical simulations were analyzed. Figure 5 compares the distribution of ethanol concentration at approximately the same location for the simulation model of this study with the study of Kwang et al.

Prior to the study of the mixing performance of the mixer, experiments were carried out for different operational simulation conditions to validate the proposed model. In this case staining was photographed in the electron microscope at fixed inlet flow rates of inlet Re = 50 and 100, respectively. Based on the experimental observations, the offset of the staining liquid representing the mixing performance was determined and compared with the molar mass fraction of ethanol at the cross section of the simulation, which was carried out using the same medium and the same flow rate conditions.

The mixing process of experimental deionized water and anhydrous ethanol can be seen in the figure from the water and stained ethanol at the inlet just in contact with the position of the staining offset degree with the simulation shown in the cross-section of the concentration is basically coincident. As the mixing length increases, under the same operating conditions, the simulation of the ethanol offset degree increases to occupy almost the entire channel, where the simulation and experimental offset distance was measured, at Re=50 can be seen from the figure were 190μm and 188μm, the degree of offset is almost the same, in the Re = 100, ethanol in the turn with the water mixing enhancement, when the Re = 100 at this time The flow pattern of the fluid changes, but through the degree of offset and the distribution of ethanol can be seen that the simulation and the experiment are also almost consistent.

In conclusion, the comparison of the numerical results with the experimental data shows that the formation of chaotic laminar flow at the notch is also well simulated in all the simulations where the mixing of ethanol and water was analyzed, and the data results of the simulations are in good agreement with the experiments. The whole mixing process can be observed and identified through experimental and numerical simulations. At Re=50 the two liquids are mixed by mutual extrusion and then by diffusion at the contact cross section, while when Re=100, the fluid flow pattern changes drastically, and all these features can be studied qualitatively by simulation, which also corresponds to the experiments, and subsequently, for the sake of research convenience and cost-saving, more microfluidic chips can be developed and optimized by simulation in order to be better applied in the nanoparticles' preparation. .

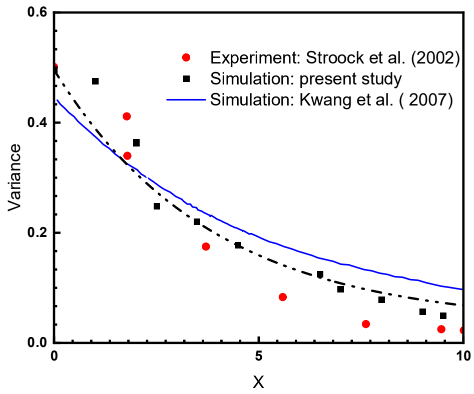

Fig.4a. Comparison of mixing coefficient simulation and experimental results.

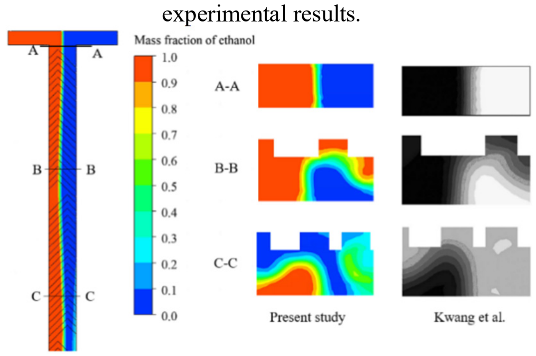

Fig.4b. Comparison of concentration simulations with Kwang's results.

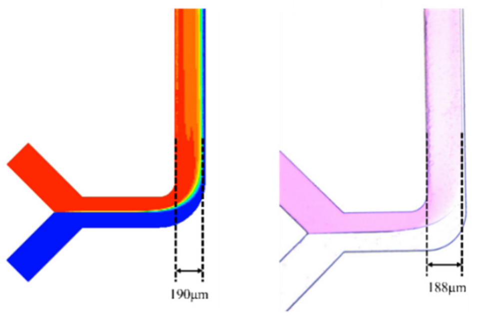

Fig.4c. Comparison of concentration simulations with experimental results. (Re=50)

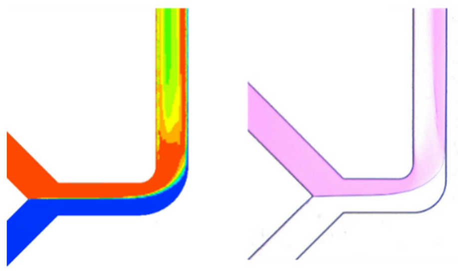

Fig.4d. Comparison of concentration simulations with experimental results. (Re=100)

3.3.Results of simulation and experimental study of mixing performance of micromixer

The size of lipid nanoparticles is strongly influenced by the mixing rate and diffusion length. Faster mixing rates result in smaller lipid nanoparticles, which is beneficial for drug delivery design. Therefore, optimizing the microfluidic device's mixing efficiency is crucial. It is important to avoid adding new content to the text.

Figure 5 shows the effect of the number of Re on the mixing performance of the SHM micromixer under different inlet conditions, with the mixing coefficient being the mixing coefficient on the cross-section at the first cycle. At Re<10, the two inlet conditions have little effect on the mixing performance of the mixer, but it is still the Y-shaped inlet that is more favourable for the preparation of lipid nanoparticles under the consideration of pressure drop.

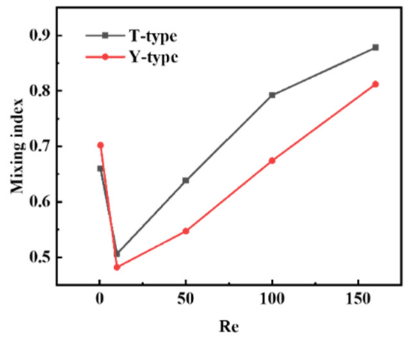

Fig. 5. Effect of different inlet structures on mixing coefficients.

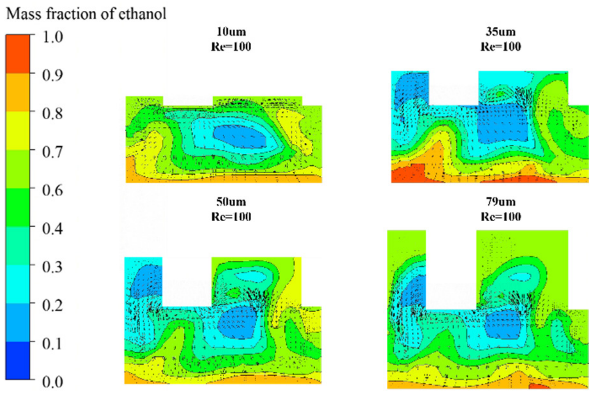

Fig.6. Mixing performance of a staggered herringbone with wavy structure at Re=100

Figure 7 illustrates the impact of notch depth on mixing. To achieve a uniform mixing index, an infinitely long channel would be required. However, due to the limited length of the channel in this case, a cross section was selected at the first loop of the SHM structure. The mixing coefficient was then derived from the mass fraction of ethanol at that location. The study shows that mixing performance improves with an increase in the depth of the notch if present. This difference is due to the varying vortex sizes produced by the herringbone notch at different depths, as reported by Wang et al. Additionally, the study highlights the impact of inlet flow velocity on convection throughout the microchannel. This study examines the effect of five different inlet flow velocities on in-channel mixing in microchannels. The velocities correspond to Re-0.5, 10, 50, 100, and 160. The mixing exponent is higher at very low Reynolds numbers, where molecular diffusion has enough time for mixing due to longer residence time. Conversely, at higher Reynolds numbers, the residence time is much faster, negatively affecting mixing performance. Therefore, the mixing performance decreases at Re=0.5-10.

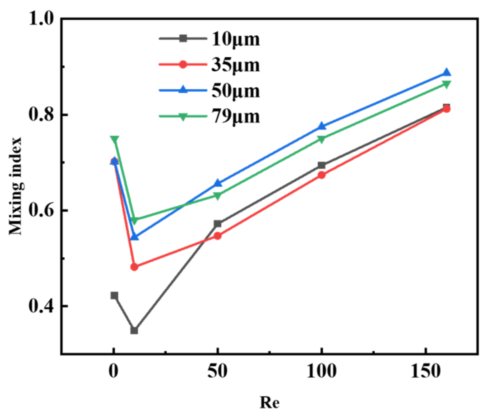

Fig.7 Mixing index distribution at 0-150 Re for staggered herringbone micro-mixer (SHM) structure with different depths.

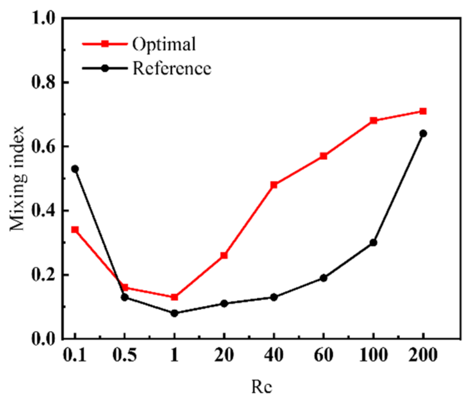

Fig.8 Comparison of mixing coefficients of optimized and conventional industrial structures at different Reynolds numbers(50μm).

The mixing performance increases gradually at Reynolds numbers higher than 10. This is due to the complex flow structure of the S-type SHM structure, which results in different flow states. The figure shows several distinct features, including different flow regimes for different inlet Reynolds numbers. It should be noted that at very low Reynolds numbers (Re~1), molecular diffusion can take place despite being in a separated flow regime due to the long residence time. As the Reynolds number increases, the flow regime changes. At Re 1-10, the flow regime is in a separated flow, and at Re ~ 50, a swirling flow regime begins to develop with secondary flows present at very low intensity. This flow regime has been found to enhance mixing performance. At Re ~ 100, the engulfing and secondary flows develop more strongly, increasing the intensity of the secondary flow and improving mixing quality. Figure 6 shows that chaotic flow regimes with relatively high secondary flow intensities develop throughout the microchannel, resulting in high-quality mixing. Thus, it can be concluded that the SHM structure improves mixing by inducing secondary flow, particularly at higher Reynolds numbers. For the preparation of lipid nanoparticles, a structure that allows fast mixing and high throughput is necessary, and based on the above study, a structure with a notch depth of 50 μm was finally selected. Although a notch structure with a depth of 79 μm also meets the requirements, the 50 μm structure has a smaller pressure drop compared to the pressure drop of the photolithographic fabrication. This makes it more conducive to the requirements of high throughput and simpler to fabricate.

Finally, we compared the mixing coefficients of the optimized structure with those of the structures used in the traditional industry. From Figure 8, it is evident that the optimized structure can mix the liquids in the channel more quickly. This faster mixing is more conducive to the preparation of smaller-sized lipid nanoparticles, providing a larger operating space for the subsequent delivery of drugs by the lipid nanoparticles [13].

4. Conclusion

Numerical and experimental analyses were conducted to optimize the microfluidics of a herringbone fluted mixer for the preparation of LNP. The goal was to enhance the mixing of two fluids by maximizing the mixing coefficient through two design variables: the depth of the notch and inlet structure. The model was validated through simulations and experiments, resulting in a model that corresponds to the experiments. The micro-mixer's optimal shape was determined through simulations. The optimization results indicated that varying the depth of the recesses improved the degree of mixing. The optimal structure for preparing lipid nanoparticles is a 50 μm notch depth. The mixing coefficients of the fluids at different Reynolds numbers also vary significantly, requiring attention during LNP preparation.

References

1. Whitesides, G.M., The origins and the future of microfluidics. Nature, 2006. 442(7101): p. 368-373.
2. Fenton, O.S., et al., Advances in Biomaterials for Drug Delivery. Advanced Materials, 2018. 30(29): p. 1705328.
3. Has, C. and S. Pan, Vesicle formation mechanisms: an overview. Journal of Liposome Research, 2020. 31(1): p. 90-111.
4. Kimura, N., et al., One-Step Production Using a Microfluidic Device of Highly Biocompatible Size-Controlled Noncationic Exosome-like Nanoparticles for RNA Delivery. ACS Applied Bio Materials, 2021. 4(2): p. 1783-1793.
5. Han, J.Y., J.N. La Fiandra, and D.L. DeVoe, Microfluidic vortex focusing for high throughput

 https://doi.org/10.1051/bioconf/202411101009

synthesis of size-tunable liposomes. Nat Commun, 2022. 13(1): p. 6997.

6. Zhigaltsev, I.V., et al., Bottom-up design and synthesis of limit size lipid nanoparticle systems with aqueous and triglyceride cores using millisecond microfluidic mixing. Langmuir, 2012. 28(7): p. 3633-40.
7. Karnik, R., et al., Microfluidic Platform for Controlled Synthesis of Polymeric Nanoparticles. Nano Letters, 2008. 8(9): p. 2906-2912.
8. Maeki, M., et al., A strategy for synthesis of lipid nanoparticles using microfluidic devices with a mixer structure. RSC Advances, 2015. 5(57): p. 46181-46185.
9. Kim, Y., et al., Mass production and size control of lipid-polymer hybrid nanoparticles through controlled microvortices. Nano Lett, 2012. 12(7): p. 3587-91.
10. Solehati, N., J. Bae, and A.P. Sasmito, Numerical investigation of mixing performance in microchannel T-junction with wavy structure. Computers & Fluids, 2014. 96: p. 10-19.
11. Stroock, A.D., et al., Chaotic Mixer for Microchannels. Science, 2002. 295(5555): p. 647-651.
12. Ansari, M.A. and K.-Y. Kim, Shape optimization of a micromixer with staggered herringbone groove. Chemical Engineering Science, 2007. 62(23): p. 6687-6695.
13. Choi, S., et al., Precise control of liposome size using characteristic time depends on solvent type and membrane properties. Sci Rep, 2023. 13(1): p. 4728.